Research Article

Tang Xuebang, Muhammad Shoaib Bhutta*, Muneeb Ahmed*, Hidayat Ullah Shah, Khalid A. Alrashidi, Saikh Mohammad, and Wail Al Zoubi*

Micro-/nano-alumina trihydrate and -magnesium hydroxide fillers in RTV-SR composites under electrical and environmental stresses

https://doi.org/10.1515/ntrev-2024-0093
received March 26, 2024; accepted August 4, 2024

Abstract: High-voltage outdoor insulating materials face formidable challenges emanating from stresses such as electrical discharge, humidity, and UV radiation, propelling them perilously toward potential failure. To combat this, researchers explored novel materials to enhance insulator performance under these stresses. In this study, samples infused with micro-/nano-alumina trihydrate (ATH) and -magnesium hydroxide (MH) were tested with a base polymer (RTV-SR – room-temperature vulcanizing silicone rubber) during a 100 h electrical discharge aging process. They were simultaneously exposed to AC discharges, UV irradiation, and varying humidity levels. The study found a decline in hydrophobicity in all samples post-discharge exposure. Notably, composites with micro- and nano-fillers exhibited prolonged hydrophobic recovery under stresses such as medium humidity and UV irradiation. Scanning electron microscopy analysis displayed deep cracks and block-like structures on surfaces, particularly in samples R_1 (50% micro-MH) and R_2 (50% micro-ATH). Aged sections of R_3 (10% nano-ATH) and R_4 (10% nano-MH) showed heightened surface cracks compared to R_5 and R_6. Energy-dispersive X-ray analysis detected surface oxidation, emphasizing the severity of electrical and other stresses. FTIR results indicated minimal absorption peak reduction in co-filled samples after aging. These findings highlight the impact of co-filled composite insulators for robust insulating systems to withstand the hostile outdoor environment.

Keywords: silicone rubber, discharge aging, hydrophobicity, magnesium hydroxide

1 Introduction

In overhead transmission and distribution lines, outdoor insulators are employed to both mechanically support the line conductors and electrically isolate them from grounded towers. To accomplish this, insulation must possess a high mechanical strength-to-weight ratio, stable thermal conductivity, high breakdown strength, and low maintenance costs [1]. Polymer coatings for insulation have advanced recently, with an emphasis on reducing flaws caused by humidity, UV light, and other environmental conditions. Despite difficulties such as environmental deterioration and electric discharge aging, polymer composites – especially those containing silicone – are preferred over ceramics because of their hydrophobic, lightweight, and long-lasting qualities [2]. The advancement of silicone rubber (SR) as an insulating material has ushered in great opportunities for operating at high voltage levels, driven by its enhanced hydrophobic properties, heightened mechanical resilience, reduced maintenance demands, and superior dielectric strength. Its hydrophobicity is a key characteristic that sets it apart from ceramic and glass insulators and contributes to its excellent pollution flashover performance [3]. When evaluating SR insulating materials in comparison to other polymers, their capacity to restore hydrophobicity emerges as a paramount attribute. The primary mechanism facilitating hydrophobicity restoration lies in the migration of pre-existing low molecular weight (LMW) polydimethylsiloxane (PDMS) from within the

* **Corresponding author: Muhammad Shoaib Bhutta**, School of Automobile Engineering, Guilin University of Aerospace Technology, Guilin, 541004, China, e-mail: shoaibbhutta@hotmail.com
* **Corresponding author: Muneeb Ahmed,** State Key Laboratory of Electrical Insulation and Power Equipment, Xi'an Jiaotong University, Xi'an, 710049, China, e-mail: ahmed.muneeb@stu.xjtu.edu.cn
* **Corresponding author: Wail Al Zoubi,** Materials Electrochemistry Laboratory, School of Materials Science and Engineering, Yeungnam University, Gyeongsan, 38541, Republic of Korea, e-mail: wailalzoubi@ynu.ac.kr
Tang Xuebang: School of Automobile Engineering, Guilin University of Aerospace Technology, Guilin, 541004, China
Hidayat Ullah Shah: Department of Physics, University of Science and Technology, Bannu, Khyber Pakhtunkhwa, 28100, Pakistan
Khalid A. Alrashidi, Saikh Mohammad: Department of Chemistry, College of Science, King Saud University, Riyadh, 11451, Saudi Arabia

material's core to the deteriorated surface. Remarkably, this transfer of LMW can occur even in cases where the insulator surface is contaminated, thus rendering SR-based insulators suitable for deployment in highly polluted environments. Due to SR's innate hydrophobic properties, it acts as a barrier against the development of leakage current, consequently deterring surface flashover [4–6]. Gubanski *et al.* examined the impact of UV radiation and surface partial discharge on different types of polymers, which include epoxy resins, RTV-SR (room-temperature vulcanizing silicone rubber), HTV-SR (high-temperature vulcanized silicone rubber), and EPDM (ethylene propylene diene monomer). They concluded that RTV and HTV-SR are more stable than other polymers [7].

In addition to all of their special attributes, SR insulators are vulnerable to aging and degradation because of their organic structure when subjected to electrical and environmental stresses [8–10]. Electrical discharges and dry-band arcing (DBA) are two types of electrical stresses that cause insulation failure. Loss of hydrophobicity causes leakage current on insulator surfaces that travels to the DBA and erodes the surface [11]. Electrical discharge is another stress that is thought to pose a risk to the effectiveness of SR insulators. The discharge's gaseous byproducts, NO and NO_2, can react with moisture to form HNO_3, which might harm both the core and the shed material. On the surface of insulators, the discharge may also generate ozone and electrons [12,13]. The type of material used to make the electrodes and the strength of the electric field at the tip both affect when the electrical discharge begins [14,15]. For instance, pointed electrodes with sharp edges produce an electric field with a high intensity and then initiate a discharge [16]. The surrounding air is ionized as a result of the strong electric field, producing ions and electrons that move in the direction of the applied electric field stress [17,18].

A variety of micro-/nano-sized fillers have been employed to enhance the characteristics of base polymeric materials in previous research studies [19–22]. These investigations have indicated that incorporating fillers improves the physical, electrical, mechanical, and thermal attributes of SR polymers. Nevertheless, it has been observed that composites containing nano-sized particles exhibit superior properties compared to micro-composites. This superiority is attributed to the larger specific surface area of nanoparticles and their enhanced interaction with the polymer [8,23]. In recent studies, the authors investigated various composites filled with micro-/nano-fillers and concluded that co-filled composites outperformed micro- and nano-filled composites [24,25].

In some other research studies, authors claimed that under electrical discharges co-filled composites performed better than micro- and nano-filled composites [26,27].

In the past, alumina trihydrate (ATH) and silica fillers have been utilized to increase the erosion resistance of SR insulating materials. Research conducted by the authors has shown that ATH nanoparticles contribute to flame retardancy, enhanced resistance to tracking, and erosion resistance, while nano-SiO_2 fillers provide increased mechanical strength to the base SR [28,29]. Meyer *et al.* studied the effects of ATH and silica fillers on SR composites with various micro-filler sizes and concentrations. They discovered that composites with 10% ATH fillers outperformed silica in terms of erosion resistance. Additionally, ATH and silica both demonstrated equal effectiveness while enhancing erosion resistance at filler loadings of 30 and 50% [28]. According to Ghunem *et al.*, ATH-filled composites demonstrated superior erosion resistance over silica-filled composites at a 50 wt% loading level and under the crucial IPT voltage [30]. However, in a different study [31], the ability of ATH and silica to halt erosion at the essential IPT voltage was the same. Using IPT, Ghunem *et al.* investigated how a 50% concentration of silica, ATH, and magnesium hydroxide (MH) affected erosion resistance. They discovered that ATH and MH filler SR composites displayed greater rates of erosion resistance than silica-filled composites due to the water of hydration [32].

Apart from DBA, electrical discharges are the other electrical stress which is the most severe and causes insulation failure. In the study, SR insulators were exposed to electrical discharges, and the authors found that the hydrophobicity of these insulators reduced over time as the ratio of water-repellent C–H, Si–CH_3, and Si–O bonds decreased and hydrophilic O–H groups and C═O bonds developed [11]. Micro-ATH and nano-alumina fillers were utilized by Nazir *et al.* to improve the characteristics of SR against electrical discharges. They discovered that the performance of SR co-filled composites against electrical discharges is greatly improved by the addition of a small amount of nano-alumina to micro-ATH [26]. ATH filled composites outperform in several cases due to the water of hydration present in it. These fillers can efficiently improve the performance of SR insulators when exposed to electrical discharge. The other filler MH also contains water of hydration, which may be a strong contender to improve SR dielectric properties, but it has not yet been explored in the realm of high voltage insulation. Research studies have shown that electrical discharges, humidity, acid fog, or vertical wind can all work together to have synergistic effects on SR insulators that hasten the breakdown of the insulator [33–35]. Sufficient research is essential to understand the synergistic effect of electrical discharge and various environmental stressors on aged SR composite materials containing varying concentrations

of ATH and MH micro-/nano-fillers. This research is crucial for mitigating the harmful effects of electrical aging on the morphology and chemical composition of SR composites, ultimately for the betterment of the comprehensive performance of SR insulation for HV insulation.

In this research, a comprehensive investigation was carried out to assess the impact of AC discharge aging on composites loaded with ATH and MH. The experiments were conducted for 100 h in a specially designed chamber, allowing for rigorous testing under controlled conditions. Six distinct types of composites were meticulously prepared, incorporating various fillers at the micro-, nano-, and micro-/nano-scales. The primary focus of this research was to delve into the long-term effects of synergistic stresses imposed on different filler types and concentrations within SR composites. A critical aspect of this investigation involved the evaluation of the hydrophobicity recovery phenomenon in the aged samples. We used advanced analytical techniques to study structural and chemical changes in both pristine and aged composites. Scanning electron microscopy (SEM) was utilized to examine the surface morphology, providing valuable visual data on the materials' microstructure. Energy-dispersive X-ray (EDX) analysis enabled the precise determination of the elemental composition, offering crucial information about the distribution of fillers and other components within the composites before and after aging experiments. Additionally, Fourier transform infrared (FTIR) spectroscopy analysis was performed to investigate the molecular changes, providing detailed insights into the chemical alterations induced by aging stresses.

2 Experimental

2.1 Material preparation

RTV-SR was used as a base material, and RTV-615A which has a density of 1.15 g/m^3 was employed. It was made up of 30% vinyl and 70% PDMS. MH and ATH were added as fillers to strengthen the basic polymer. To accomplish adequate deagglomeration, filler particles were first agitated for 15 min in a 100 ml solution of ethanol before being subjected to ultrasonication for 30 min. After that, RTV-615A was added to the filler, and the mixture was blended for 15 min with an HSM-100 LSK high-shear mixer. After that, the mixture was agitated for a further 15 min before the curing agent (RTV-615B) was added. The ratio of Parts A to B was maintained at 10:1. The resulting mixture was subsequently dried for 10 min in a vacuum desiccator to release any trapped air. The prepared solution was then poured into steel molds for the required shape and dimension. The shape was flat, and the dimensions were 120 mm × 50 mm × 5 mm. The vulcanization process was finally completed by applying 30 MPa of pressure using a hydraulic press for 30 min, followed by 4 h of post-curing in an oven heated to 85°C. Table 1 presents the details of the RTV-SR composites that were employed in this study. ATH and MH were the fillers utilized. Rectangular samples with dimensions of 120 mm length, 50 mm width, and 5 mm thickness were employed.

Table 1: Sample notations with base polymer and filler percentages

Sample notation	RTV (%)	Micro-filler	Nano-filler
R_1	50	50% ATH	—
R_2	50	50% MH	—
R_3	90	—	10% ATH
R_4	90	—	10% MH
R_5	70	25% ATH	5% ATH
R_6	70	25% MH	5% MH

2.2 Electrical stress aging setup

Electrical discharge was produced using a point-to-plane copper electrode arrangement. The arrangement was contained in a stainless-steel chamber with a controlled gaseous atmosphere, as shown in Figure 1. The point electrode has a 2 mm tip diameter and acts as a discharge source [36]. The test sample is placed on the bottom round plate electrode, which has dimensions of 50 mm in diameter by 10 mm in thickness and is connected to the ground.

Figure 1 illustrates an outline viewpoint and image of the electrical aging setup. Electrical charge was applied to the test samples using 6 single needles, simple electrodes, and a 16 kVA transformer. With the aid of an HV probe with a 1,000:1 ratio that was attached to an oscilloscope, a high voltage was applied. The test samples were exposed to 10 kV, while the voltage was adjusted by a variac. Additionally, UVA 340 lamps were used to provide UV radiation, a humidifier with a sensor, display, and controller was utilized in the chamber to manage the level of humidity, and a circuit breaker was also connected in case of any fault. Three samples of each type were evaluated for repeatability of results till 100 h with 10 kV applied to the samples. The distance between the needle tip and the sample was maintained at 1 mm with the help of a standard gauge block [26,37]. Samples were also examined under the impact of UV radiation. Experiments were performed at two different relative humidity levels, medium (55–65%) and

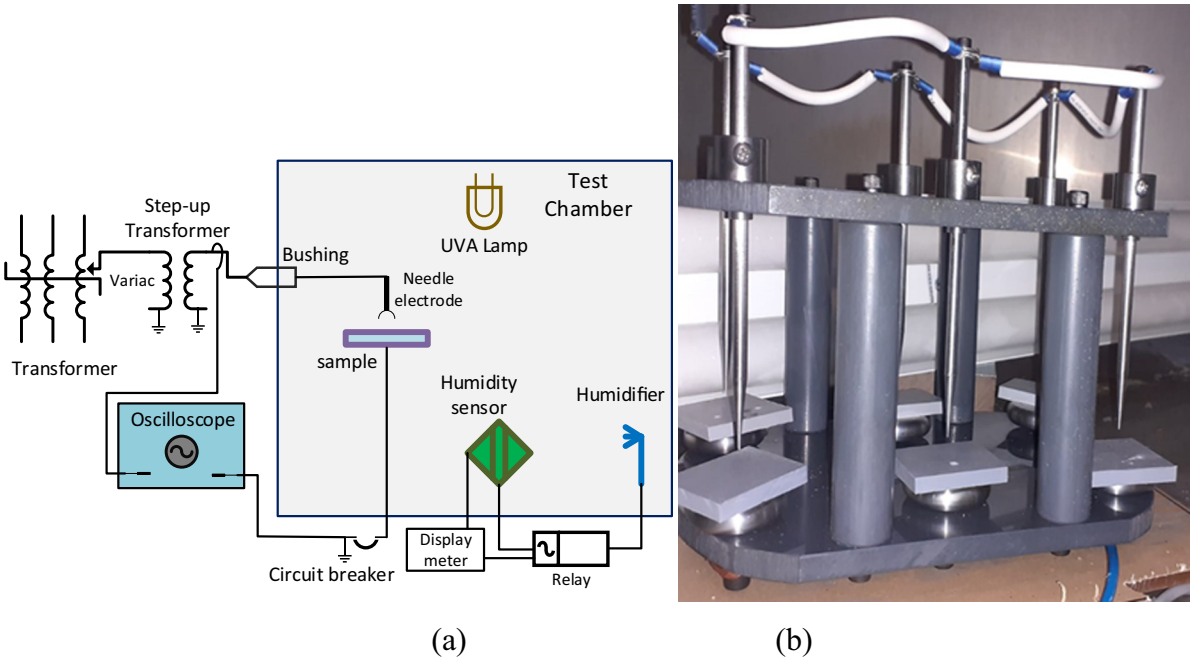

Figure 1: Experimental setup of electrical stress causing degradation. (a) Schematic view. (b) Photographic view of needle-plane electrodes.

high (75–85%). De-ionized water was used to fill the humidifier to protect the system from breakdown due to ionization in the chamber's environment.

2.3 Hydrophobicity loss and recovery analysis

Since the aging process begins with the loss of hydrophobicity, it is imperative to evaluate SR's hydrophobicity. To quantitatively assess the hydrophobicity loss and recovery, a variety of methods can be used, such as water soaking, sliding angle, dynamic contact angle, static contact angle, and the Swedish Transmission Research Institute scale. Measuring the static contact angle, which exists at the point where a liquid drop touches a material surface, is the most common way to determine them. The relationship between the contact angle, solid surface energy, and liquid surface tension is described by the Young–Dupré equation as follows:

$$\gamma_{GS} = \gamma_{SL} + \gamma_{LG}\cos\theta, \tag{1}$$

where γ_{GS}, γ_{SL}, and γ_{LG} represent the interfacial tension between the gas and solid, the solid and liquid, and the liquid and gas, respectively, and θ represents the contact angle.

Hydrophilic materials enable the water to touch more surfaces because of their high surface energy and ease of wetting, and as a result the contact angle eventually drops from 90°. Contrarily, water cannot flow across the surfaces of hydrophobic materials due to their low surface energy, resulting in a contact angle of larger than 90° [38]. The contact angle of SIR-aged composites was measured using a micropipette with a drop size of 20 µL. De-ionized water was dropped onto the SIR surface, which was being aged just below the needle tip. Then, each droplet was photographed and uploaded to a computer. To determine the static contact angle of each droplet, "ImageJ" software with the low-bond axisymmetric drop shape analysis (LBADSA) technique was utilized [39]. Contact angles of aged samples were determined immediately following the aging through 100 h with various intervals of time to understand the hydrophobicity recovery phenomenon.

2.4 Morphological analysis

Morphological analysis was performed by scanning electron microscopy (SEM). The surface topography data can be gathered to detect morphological changes in the tested surfaces. High-energy electron beams were used to scan the sample in a raster scanning pattern to produce SEM micrographs. The electron beam interacts with the surface atoms of the sample to produce signals that reveal information about surface topography and composition. To create high-quality SEM micrographs and determine the elemental compositions on the surface of discharge-aged

materials, an FEI Quanta FEG 250 ESEM system, which also has an EDX detector, was employed.

2.5 FTIR analysis

In-depth analysis of the functional chemical groups within the studied materials was carried out with the powerful tool of FTIR spectroscopy. This technique meticulously examined absorbance peaks spanning a spectral range from 500 to 4,000 cm^{-1}. The data captured from both the weathered, aged samples and the pristine, unaged counterparts were rigorously compared. This meticulous comparison served as a beacon, illuminating the extent of degradation inflicted by relentless environmental stresses.

3 Results and discussion

3.1 Hydrophobicity loss

All samples had their contact angles assessed both before and immediately after the discharge aging test, which lasted for 100 h. All untreated samples had contact angles greater than 90°, which indicates good hydrophobicity before testing. Regardless of the type or quantity of fillers used, the samples lost their hydrophobicity because of prolonged discharge exposure and other applied stresses. Table 2 displays the measured contact angles for each sample at the beginning (untreated) and immediately following the aging experiment.

The aged sample's contact angles demonstrate that UV has a higher effect on hydrophobicity. Additionally, compared to medium humidity, the loss in contact angle was a little bit larger at high humidity. For samples R_1, R_2, R_3, and R_4, Table 2 clearly shows that high humidity had a significantly greater impact on hydrophobicity loss. The contact angles of co-filled samples R_5 and R_6 were greater than those of R_1, R_2, R_3, and R_4, indicating that the co-filled composite had greater hydrophobicity. Under humidity and without UV, samples R_5 and R_6 performed better, with contact angles of 36.6° and 35.2°, respectively. Moreover, samples filled with ATH had higher contact angles after an aging period, and the co-filled sample R_5 showed the highest hydrophobicity in all cases. Figure 2 shows the pictures of droplets on the surface of aged samples showing loss of hydrophobicity.

3.2 Hydrophobicity recovery

The ability of SR insulators to regain their hydrophobicity is a special quality, and a thorough analysis of the behavior was done to adequately pinpoint the causes of recovery of older composites. Due to the initial rapidity of the recovery, the contact angles for aged samples were first assessed at shorter intervals. To ensure consistency, we acquired three photos of each composite and averaged the contact angle values. Four separate cases were examined, and after aging of the samples, 1,296 images of droplets were captured using a high-resolution camera. Then, the recovery phenomena of the samples were examined using ImageJ software. Figures 3 and 4 show the difference in contact angles for all six filled composites under medium/high humidity levels, with or without UV radiation and at a 1 mm electrode–sample distance.

After 30 min of recovery time, the recorded increase in contact angles of samples aged under high humidity and UV radiation was 11.3°, 17.9°, 13.3°, 9.6°, 8.6°, and 4.7° for samples R_1, R_2, R_3, R_4, R_5, and R_6, respectively. The difference in contact angles after 40 h of recovery time was 43.2°, 42.7°, 42.1°, 39°, 43.4°, and 36.6° for samples R_1, R_2, R_3, R_4, R_5, and R_6, respectively. The recovery rate was the highest for sample R_5 when exposed to high humidity and UV radiation. Under the influence of UV radiation and high humidity, the contact angles recorded were 66.3°, 65.8°, 71.1°, 69.6°, 78.7°, and 73.6° for samples R_1, R_2, R_3, R_4, R_5, and R_6, respectively, after 100 h of recovery time.

Table 2: Contact angles of samples before and immediately after discharge aging

Samples	Untreated	High humidity (UV)	Medium humidity (UV)	High humidity (without UV)	Medium humidity (without UV)
R_1	98.6°	20.2°	21.6°	21.7°	22.4°
R_2	97.8°	13.7°	20.4°	18.9°	20.8°
R_3	101.3°	25.1°	28.1°	27.1°	30.1°
R_4	99.6°	24.5°	26.8°	26.5°	28.2°
R_5	102.5°	29.3°	35.9°	30.2°	36.6°
R_6	101.6°	28.6°	33.4°	29.9°	35.2°

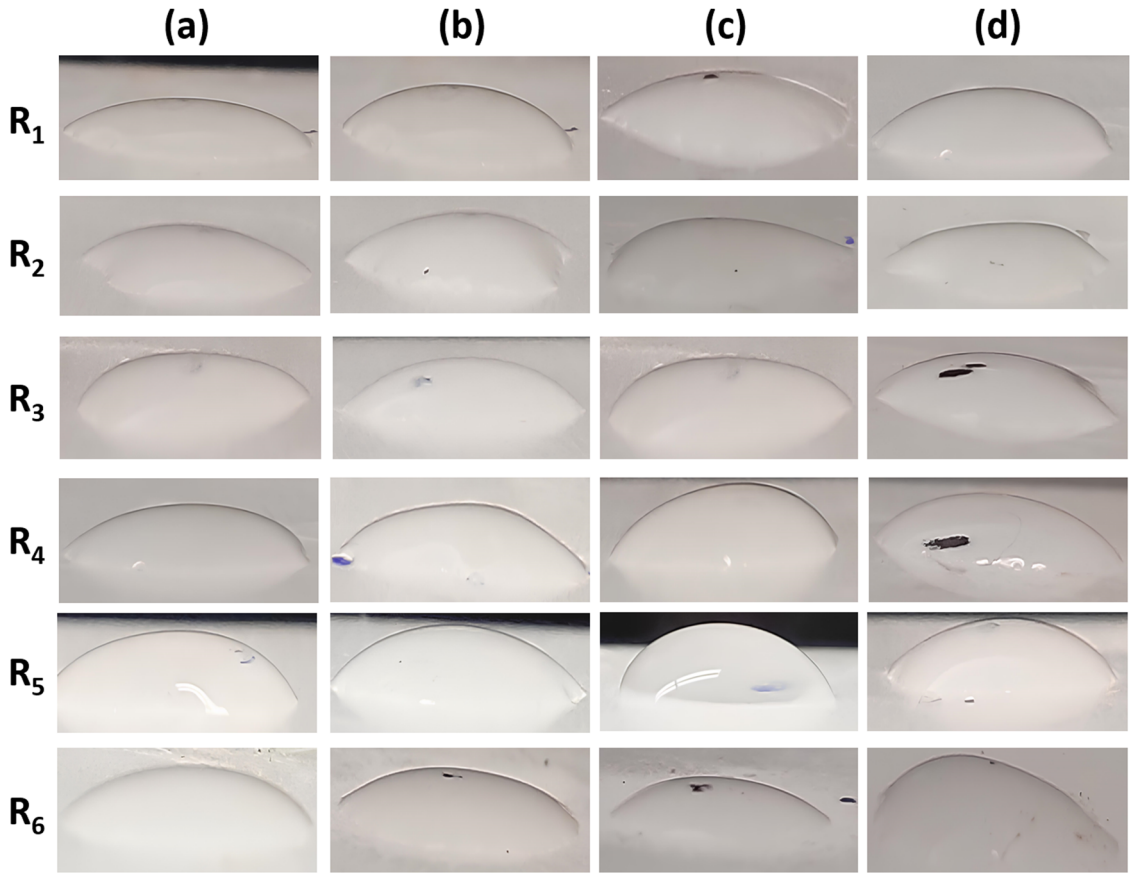

Figure 2: Images of droplets on the surface of samples after discharge aging experimentation under: (a) UV irradiation and high humidity, (b) without UV irradiation and high humidity, (c) UV irradiation and medium humidity, and (d) without UV irradiation and high humidity.

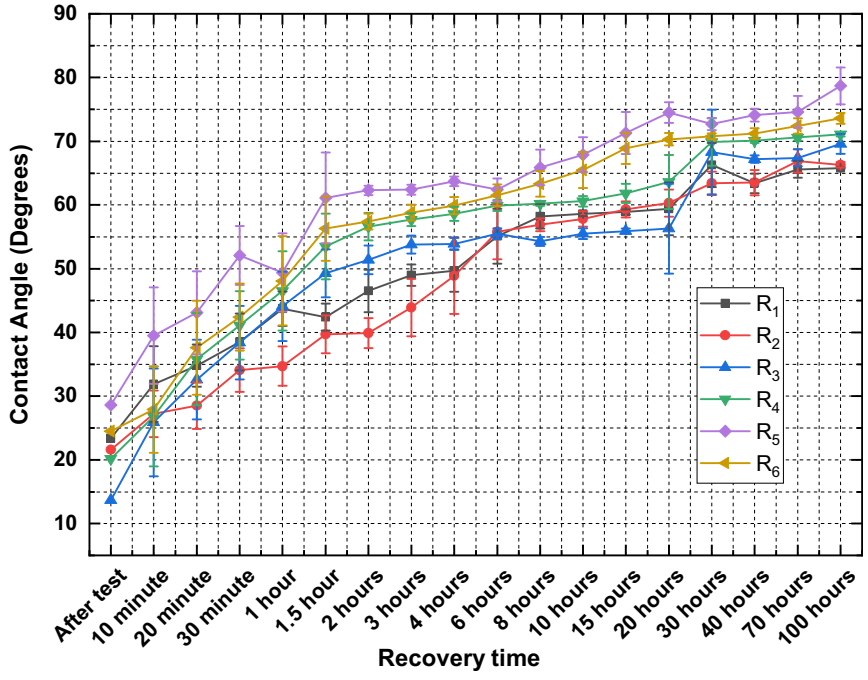

Figure 3: Hydrophobicity recovery of electrical stress exposed composites under high humidity and UV irradiation.

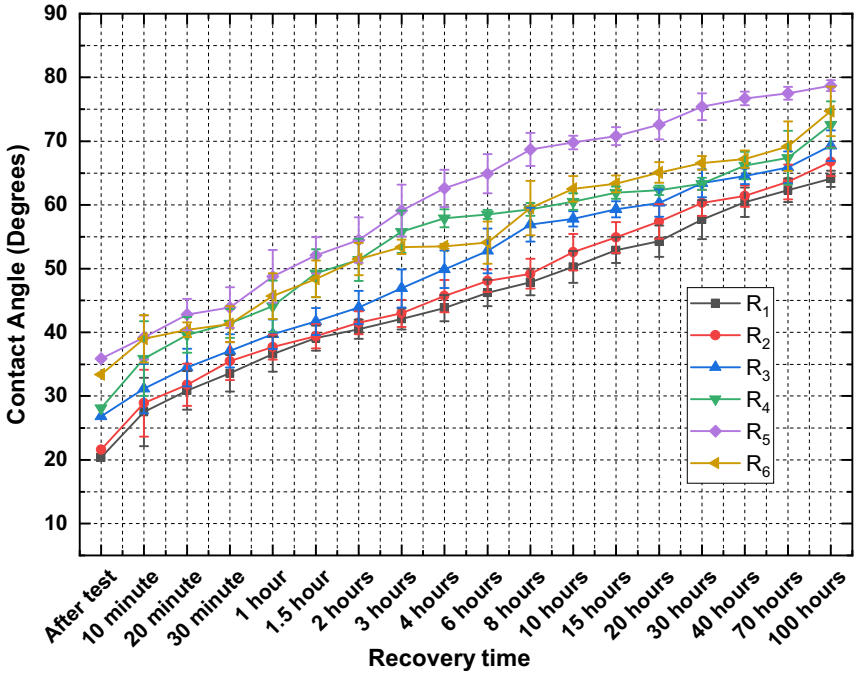

Figure 4: Hydrophobicity recovery of electrical stress exposed composites under high humidity and without UV irradiation.

In the case of ATH fillers, the contact angles recorded were higher than those of MH filled composites. However, the micro-filled composites showed the least recovery after 100 h when exposed to discharge aging. From Figures 3 and 4, it can also be seen that the composites co-filled with micro/nano-filler concentration showed a faster recovery rate from the start up to 100 h of recovery time. Figure 5 shows the curves of all samples that were exposed to discharge, UV radiation, and medium level of humidity. It is quite obvious that the loss of hydrophobicity was higher in the case of high humidity, but looking at the recovery phenomenon it was slower in the case of medium humidity level during 100 h of recovery time.

We also found that the impact of UV radiation along with discharge exposure causes more degradation on the surface of all composites. The recovery rate was also slower in all samples because of the impact of UV radiation. Figures 5 and 6 show the curves of hydrophobicity recovery for samples that were aged under discharge, medium humidity level, UV irradiation, and without UV irradiation. It can be seen that the recovery rate was slower from the start till the end of 100 h of recovery time than in the case of high humidity level.

The contact angles recorded for sample R_5 after 100 h of recovery were 72.7° and 75.7° under medium humidity level, UV radiation, and without UV radiation exposure, respectively. The other co-filled sample R_6 had a faster recovery rate than micro-filled and nano-filled composites showing its better recovery rate. From Figures 5 and 6, it can be seen that the recovery rate is the fastest in the case of co-filled composites and slowest in the case of micro-filled composites. The filler type and concentration also had a major role in the case of hydrophobicity recovery rate. The loss of hydrophobicity was more in the case of samples filled with MH fillers, micro-fillers, and nano-fillers. Whereas the ATH filler and co-filled composites experienced the least amount of hydrophobicity loss and recovered more quickly. The synergetic impact of electrical discharge along with UV irradiation and humidity showed a damaging impact on the composite's surface, and the contact angles of all composites never recovered back to 90°. This shows the severity of electrical discharge, humidity, and UV irradiation on the surfaces of composites having different concentrations of fillers.

3.3 SEM analysis

SEM micrographs show that the portions of the SR samples that were directly underneath the high-voltage electrode underwent surface deterioration. The samples R_1, R_2, R_3, R_4, R_5, and R_6 were put to test under various humidity levels, UV rays, and electrical discharge application at a 1 mm distance. Figure 7 demonstrates that the degraded surfaces of R_1 and R_2 subjected to UV irradiation, high humidity, and electrical discharge show a higher degree of deterioration

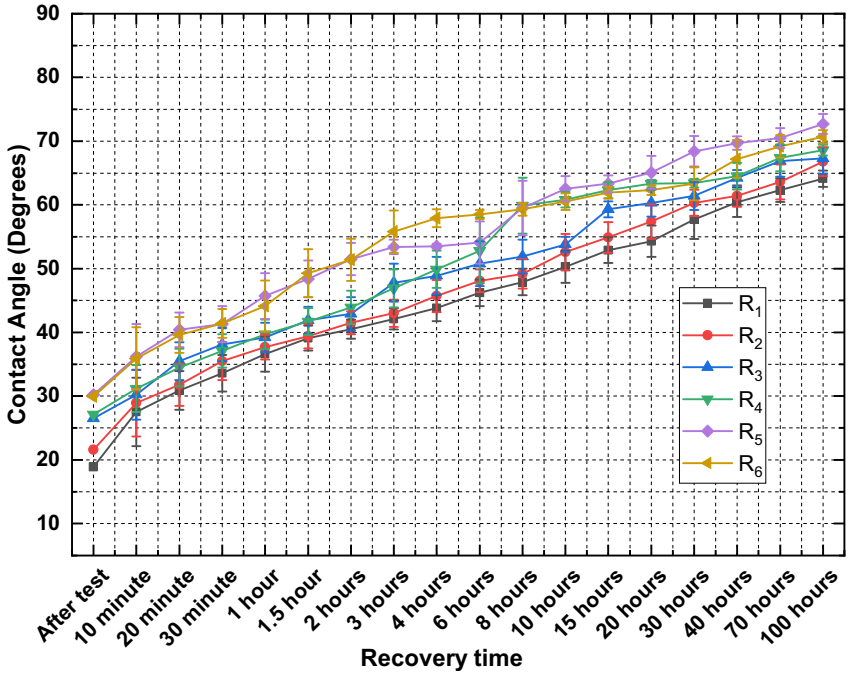

Figure 5: Hydrophobicity recovery of electrical stress exposed composites aged under UV irradiation and medium humidity level.

and more cracks. High humidity levels and UV irradiation caused more deep fissures and cracks to appear on R_1 and R_2 surfaces than they did at medium hydrophobicity, which results in a loss of hydrophobicity. The deterioration of the aged portion of R_3 at various humidity levels is depicted in Figure 7. The size of the cracks was larger at high humidity levels and UV irradiation for samples R_1 and R_2 having only micro-fillers. Samples treated under medium humidity level and UV radiation recorded smaller cracks. Additionally, the surface of samples treated without UV

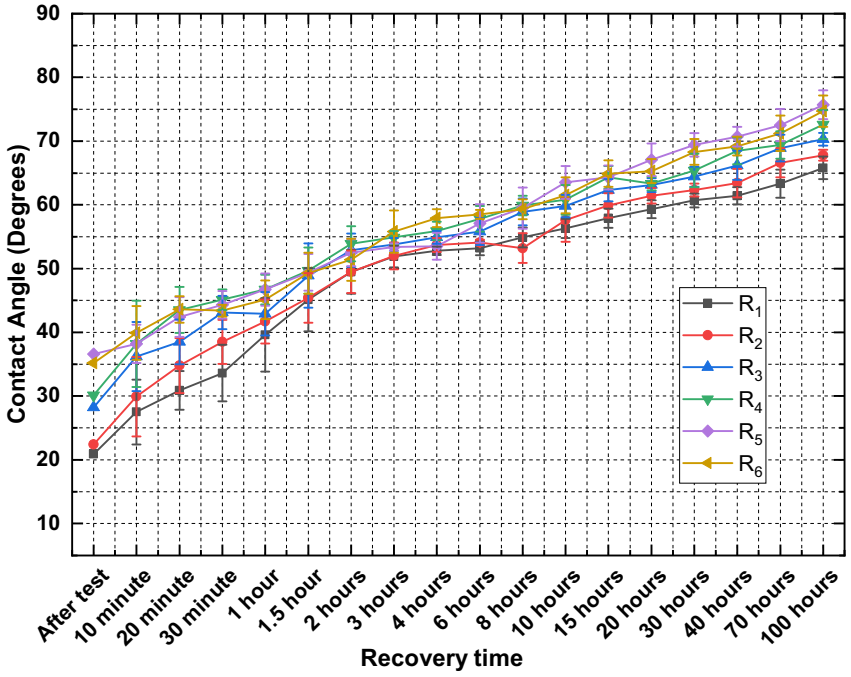

Figure 6: Hydrophobicity recovery of electrical stress exposed composites aged under medium humidity and without UV radiation exposure.

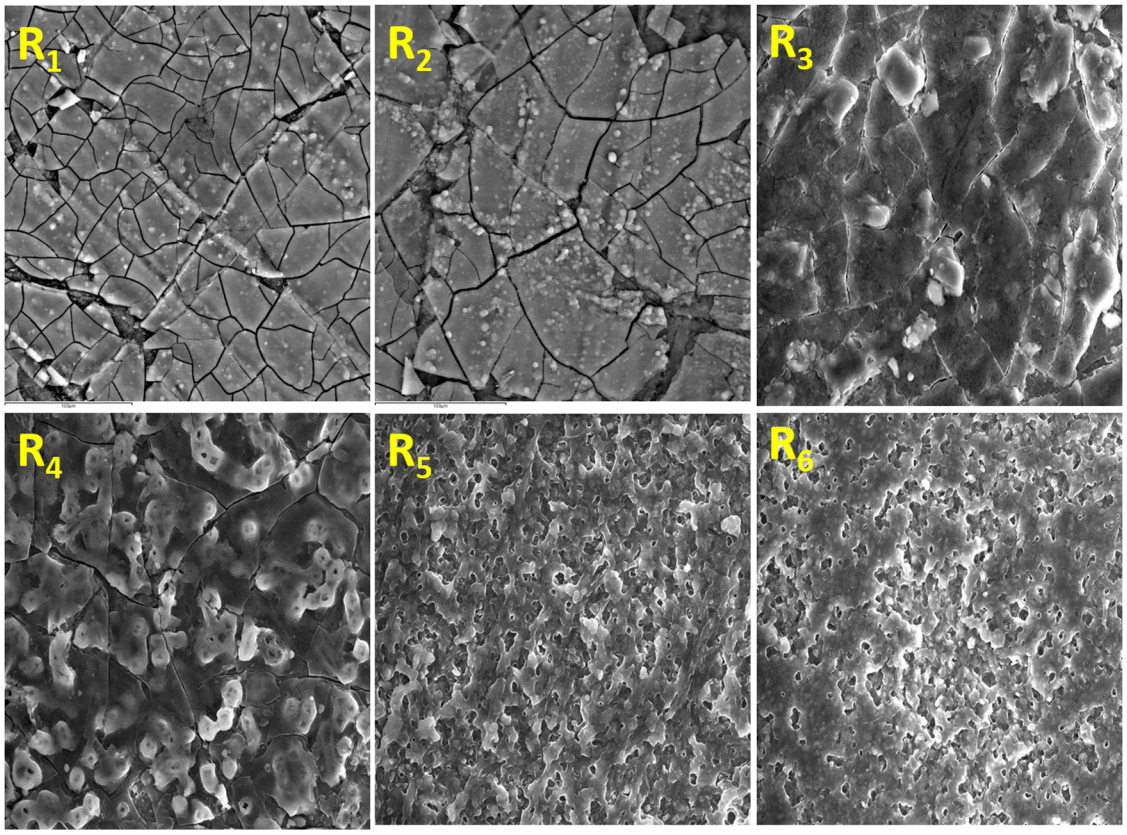

Figure 7: SEM micrographs of composites treated under electrical discharge, high humidity, and UV irradiation.

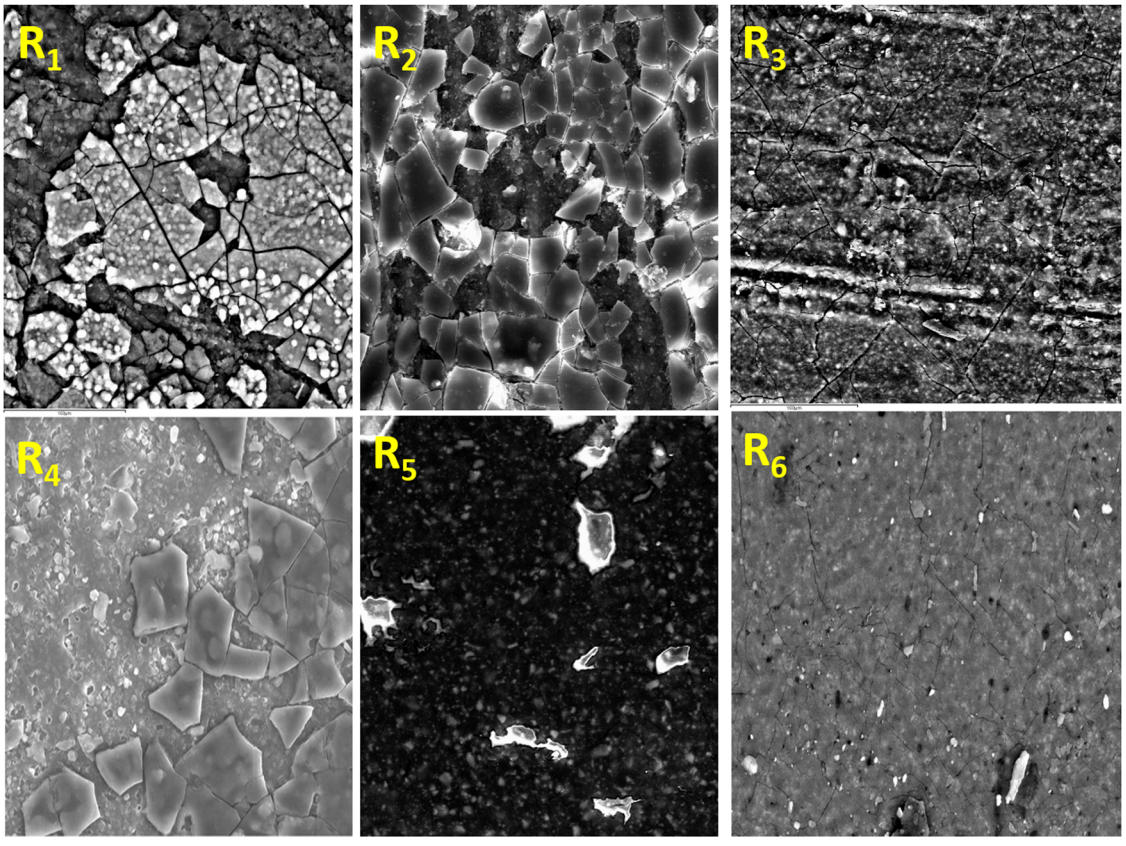

Figure 8: SEM micrographs of composites exposed to electrical discharge, medium humidity, and UV irradiation.

radiation similarly exhibited electrical discharge and caused deterioration, although the surface morphology was superior to that of samples exposed to UV light.

Under high humidity and UV exposure, sample R_2 displayed significant degradation that led to larger fissures and a block-looking structure. Additionally, as seen in Figure 8, sample R_2 at a medium humidity level with UV exposure showed higher degradation with cracks, a blocky structure, and white powder on its surface than other samples. In every situation, the surface morphology of the R_5 (25% ATH + 5% nano-ATH) and R_6 (25% MH + 5% nano-MH) treated areas produced improved outcomes that are also consistent with the earlier hydrophobicity recovery results. In comparison to samples R_3 and R_4, the treated portion of sample R_4 showed significant deterioration at medium humidity level and under UV radiation. Additionally, R_4 displayed deeper fissures, a blockier structure, and white powder when tested under UV radiation and at medium humidity. Due to the damaging effects of electrical discharge, humidity, and UV radiation, samples R_1, R_2, R_3, and R_4 showed a higher degree of degradation than R_5 and R_6 composites. In every instance, it appears that the UV rays

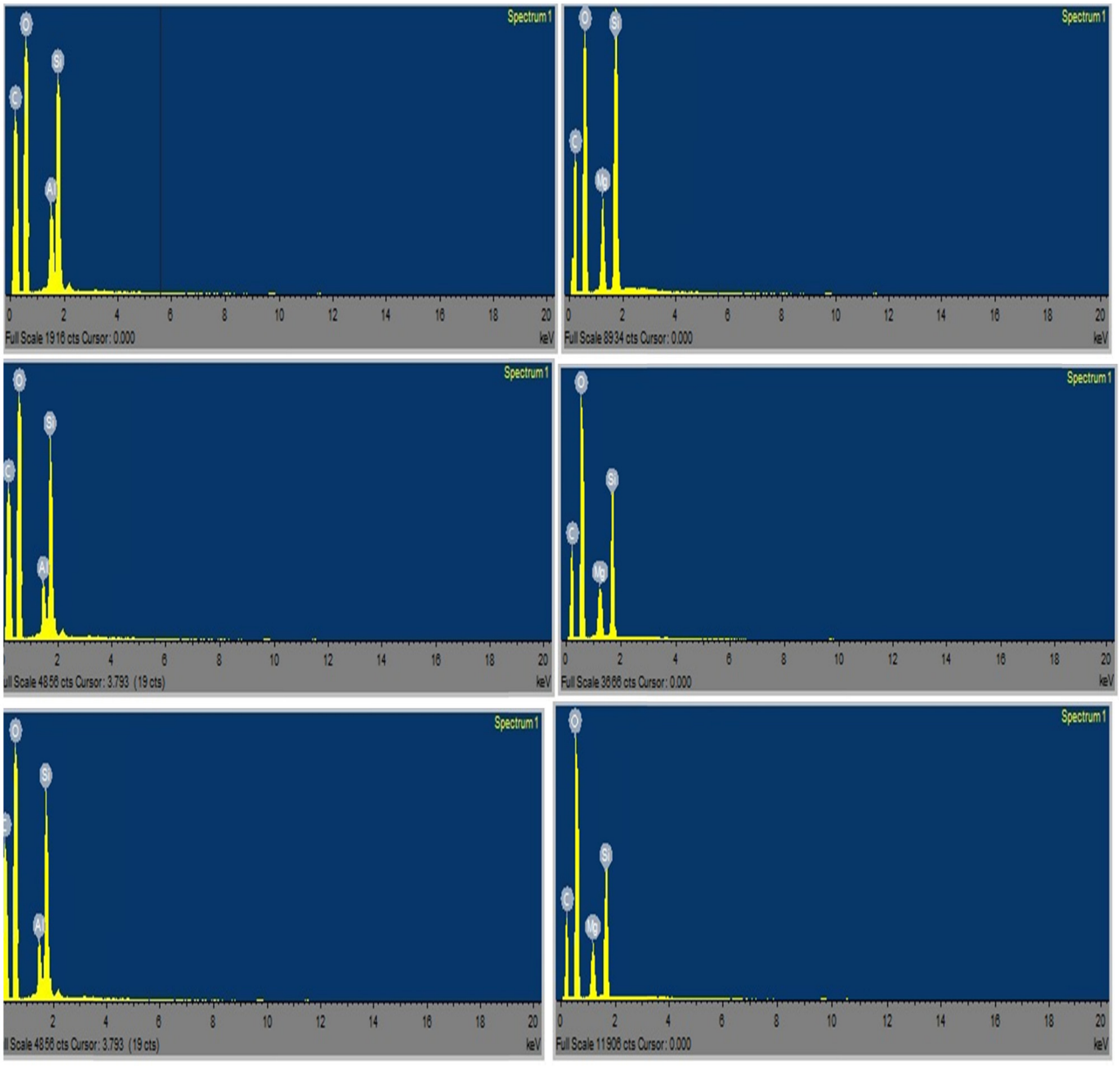

Figure 9: EDX analysis to identify changes in various composite components – silicon (Si), oxygen (O), carbon (C), aluminum (Al), and magnesium (Mg).

Table 3: Elemental composition of stress-aged composites (50% micro-filler concentration)

R_1	%C	%O	%Al	%Si
Unaged	20.91	38.96	16.38	23.74
Without UV radiation and high humidity	18.35	47.15	10.30	24.20
With UV radiation and high humidity	16.66	50.59	7.69	25.06
Without UV radiation and medium humidity	18.55	46.01	10.78	24.66
With UV radiation and medium humidity	16.10	50.32	8.83	24.75
R_2	%C	%O	%Mg	%Si
Unaged	23.65	32.32	17.16	26.87
Without UV radiation and high humidity	22.98	35.96	13.62	27.44
With UV radiation and high humidity	17.52	42.77	9.79	29.92
Without UV radiation and medium humidity	23.11	35.21	14.19	27.49
With UV radiation and medium humidity	17.37	42.30	10.69	29.64

are more harmful, causing deep fissures and the development of white powder on the surface.

3.4 EDX analysis

Before and after the discharge test, EDX analyses were conducted to identify changes in various composite components. Silicon (Si), oxygen (O), carbon (C), aluminum (Al), and magnesium (Mg) are the main components of composites as shown in Figure 9.

The samples were examined at a distance of 1 mm under various humidity conditions, UV light, and without UV light. The elemental compositions of untreated and stress-aged 50% filled composites under various circumstances are shown in Table 3. After aging, samples R_1 and R_2 revealed a reduction in their filler content, with the largest reduction reported from 16.38 to 7.69%, indicating a loss of more than 50% under conditions of high humidity and UV exposure. Under various humidity levels, samples R_1 and R_2 demonstrated an increase in the oxygen level while experiencing a drop in silicone and filler contents. After aging, sample R_2 likewise showed a reduction in filler content; under high humidity and medium humidity with UV exposure, the Mg reduction was noted to be 17.16–9.79% and 10.69%, respectively. Additionally, it was observed in all cases that the silicone and oxygen levels had increased. Spectra of samples R_1 and R_2 are shown in Figure 9, illustrating the impact of stress, high humidity, and UV radiation on the reduction of filler content and increase in the oxygen level due to the oxidation process.

The chemical constituents of samples R_3 and R_4 that were exposed to high humidity, medium humidity, UV radiation, and without UV radiation are shown in Table 4. For sample R_3, the loss of aluminum content was the greatest when exposed to high humidity and UV radiation, demonstrating the severity of the discharge effect and the additive effects of humidity and UV radiation on the filler concentration. Under conditions of high humidity and UV radiation, the proportion of O for sample R4 on the surface increased from 35.45 to 39.85%. This demonstrates the auto-

Table 4: Elemental composition of stress-aged composites (10% nano-filler concentration)

R_3	%C	%O	%Al	%Si
Unaged	25.70	34.92	4.96	34.42
Without UV radiation and high humidity	23.33	36.75	4.35	35.57
With UV radiation and high humidity	22.39	38.06	3.75	35.80
Without UV radiation and medium humidity	23.85	35.79	4.66	35.70
With UV radiation and medium humidity	22.92	37.15	4.22	35.71
R_4	%C	%O	%Mg	%Si
Unaged	24.84	35.45	5.82	33.89
Without UV radiation and high humidity	22.24	37.64	4.57	35.55
With UV radiation and high humidity	19.85	39.85	3.96	36.34
Without UV radiation and medium humidity	22.35	37.33	4.85	35.47
With UV radiation and medium humidity	20.96	38.47	4.35	36.22

oxidation and development of OH hydrophilic groups on the sample's surface [40].

The percentage increase in silicone for samples R_3 and R_4 shows the recovery phenomena because of the movement of LMWs on the surface of the samples. Due to the synergistic effects of stresses, samples R_5 and R_6 of co-filled composites also displayed an increase in oxygen content and a decrease in the percentages of silicon and carbon (Table 5). Under conditions of high humidity and UV radiation, the sample R_6 with micro-MH + nano-MH also showed a drop in Mg from 13.36 to 7.72%. Additionally, the concentration of silicon and oxygen was increased, demonstrating how LMWs diffused throughout the sample's surface. The sample R_5 showed the least amount of filler content loss across all cases, and the recorded oxygen level was not particularly high, indicating less oxidation on the surface of this co-filled composite.

3.5 FTIR analysis

The aged and unaged samples were tested using attenuated total reflection (ATR) mode Fourier transform infrared (FTIR) spectroscopy. The samples were tested under the following conditions: un-aged, medium humidity without UV mode, high humidity without UV mode, and high humidity with UV mode. The FTIR spectra of R_2, R_3, and R_5 are presented in Figure 10. Figure 10(a) shows the decrease in absorption peaks of sample R_2 along with associated functional groups.

Each peak in the graph displays the corresponding wavenumbers in FTIR spectra. The hump-shaped peak in aged composites between 3,200 and 3,300 cm^{-1} indicates the presence of hydrophilic H bonded OH stretch, which emerged because of electrical stress treatment. In comparison to deteriorated R_5, the increase in OH peak heights in degraded R_2, and R_3 is relatively significant. The peak at 2,962 cm^{-1} deviates from the virgin state values by 76.5, 66.5, and 35.2%, respectively, and reveals CH stretch in CH_2 and CH_3 in the spectra. In comparison to its virgin value, the degraded R_2 shows a higher drop of 17%.

The functional groups CH and NO (nitro) are represented by the peak heights at 1,413 and 1,350 cm^{-1}, respectively. After electrical stress exposure, both functional groups' peak heights significantly increase. Additionally, all aged composites exhibit a substantial increase in the absorbance intensity of the nitro group, indicating the presence of nitride compounds on the deteriorated composites [41]. The Si–O–Si is discovered to be more stable in R_5 (25% micro-ATH + 5% nano-ATH) than in R_3 (10% nano-ATH), in contrast to Si-CH_3. As a result of electrical stress exposure, Si $(CH_3)_2$ in the composites has been severely damaged, as shown by a dramatic decrease in peak heights at 787 cm^{-1} in Figure 10. The decrease in Si $(CH_3)_2$ absorbance intensities is discovered to be in the same order as the Si–O–Si main chain of composites. In all composites, there is a little increase in the Si $(CH_3)_3$ absorption intensity. In damaged R_2, Si $(CH_3)_3$ peak heights increased by 16% but only by 8% and 5 in R_3 and R_5, respectively. This suggests enhanced Si $(CH_3)_3$ deformation resistance provided by R_3 and R_5. There was a noticeable decrease in absorption peaks of all samples because of the applied stresses. The samples treated under high humidity and UV irradiation caused more degradation than in other conditions. Moreover, the co-filled composite R_5 showed less increase in its absorption peaks when tested under electrical stress, UV irradiation, and high humidity conditions which validates our previous results.

4 Discussion

The important findings of hydrophobicity recovery studies on different composites under different environmental

Table 5: Elemental composition of stress-aged composites (5% nano-filler and 25% micro-filler concentration)

R_5	%C	%O	%Al	%Si
Unaged	23.68	33.02	12.08	31.22
Without UV radiation and high humidity	20.36	36.95	9.72	32.97
With UV radiation and high humidity	19.75	39.28	7.29	33.68
Without UV radiation and medium humidity	21.05	36.37	9.88	32.70
With UV radiation and medium humidity	20.02	38.25	8.67	33.06
R_6	**%C**	**%O**	**%Mg**	**%Si**
Unaged	21.58	34.36	13.36	30.70
Without UV radiation and high humidity	18.78	38.93	10.34	31.95
With UV radiation and high humidity	17.11	41.63	7.72	33.54
Without UV radiation and medium humidity	18.91	38.39	10.82	31.88
With UV radiation and medium humidity	18.04	40.68	8.33	32.95

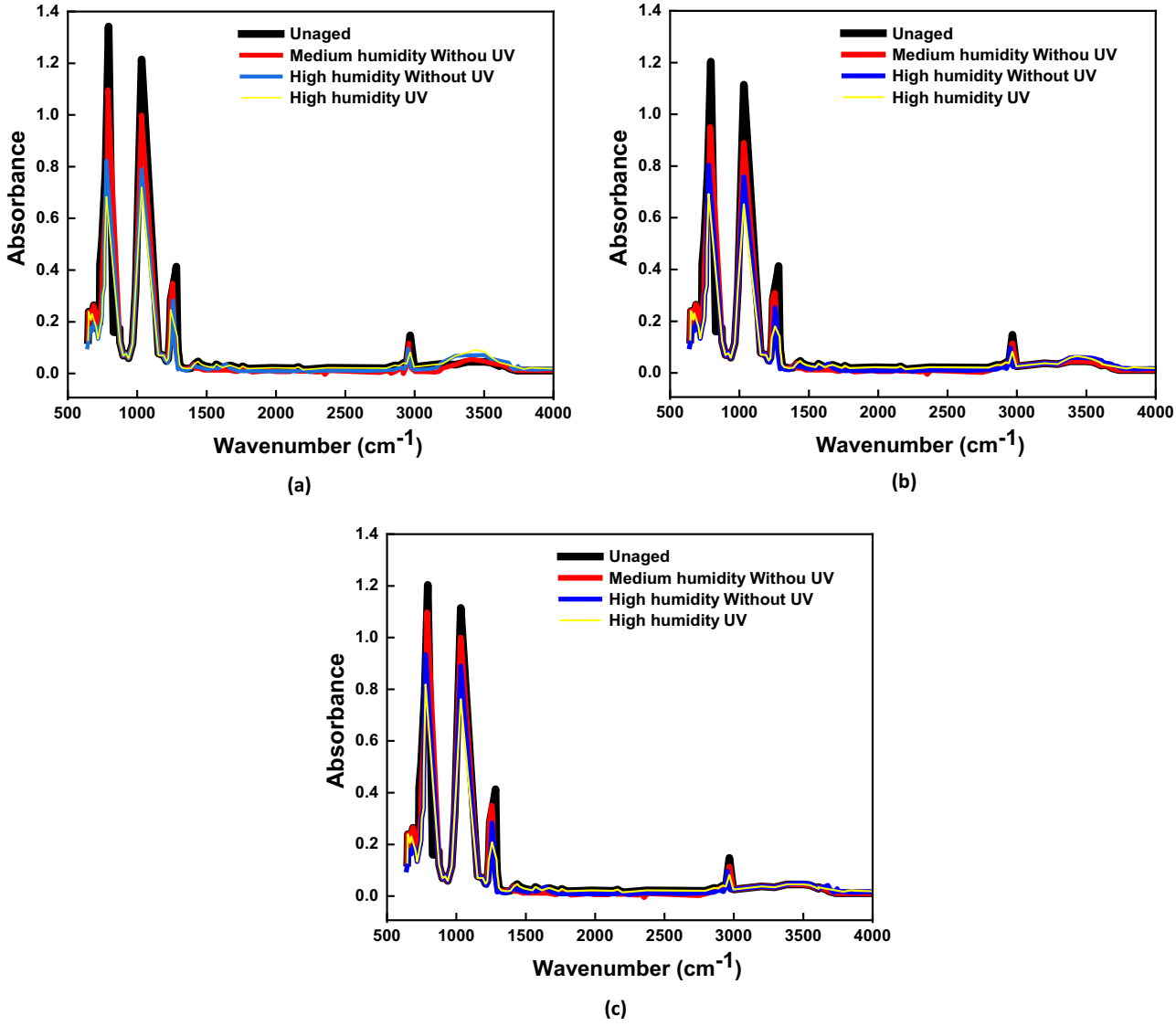

Figure 10: FTIR spectra of aged and unaged samples illustrating the functional groups under different stresses: (a) R_2, (b) R_3, and (c) R_5.

conditions and electrical stress exposure are noticed. The samples having both micro- and nano-fillers showed faster recovery than samples filled with micro-fillers and nano-fillers. This might be a result of easier LMW component transit from the bulk to the surface in co-filled composites. The higher filler concentrations in 50% micro-filled composites may serve as a barrier that slows down the diffusion of LMW components. Moreover, because of electrical discharges, an increase in oxygen content was also noticed on SR's surface, which causes the development of a hydrophilic layer that resembles silica and polar silanol groups on the PDMS surface. Severe oxidation, according to the mechanism outlined in the study of Hillborg and Gedde [42], transforms the hydrophobic $–CH_3$ groups to $–CH_2$ and produces hydroxyl ($Si–CH_2OH$) and peroxides ($Si–CH_2OOH$) as a result of a reaction between the oxygen content and PDMS. Higher electrical discharge intensities below the needle tip may cause more severe surface oxidation and the development of hydrophilic layers. Additionally, the hydrophobicity recovery phenomena after electrical stress exposure are attributed to the polar group reorientation, condensation of silanol groups, and the migration of LMW components from the bulk to the surface of PDMS [18].

The contact angles had lower values under the influence of UV radiation for all types of composites which showed the increase in severity of the test because of UV radiation. Another important finding of this study is that at the start just after aging most samples had the highest recovery of contact angle only after 10 min of recovery time. That is why, we took a lot of images during the first

hour of recovery time. After 10 h of recovery time, the contact angles of all composites had a marginal increase in their values. Moreover, the impact of humidity level also showed that at lower values of humidity, the recovery of hydrophobicity was slower than that at higher levels of humidity. Samples R_5 and R_6 showed better results than samples R_1, R_2, R_3, and R_4 tested under different conditions.

Figures 7 and 8 depict the micrographs of aged areas of composites showing cracks, pits, block type structure, and white powder because of the impact of electrical stress and other applied stresses. The development of surface cracks may contribute to higher contact angle recovery because these defects enable LMW constituents of PDMS a less-resisting route to diffuse from the bulk to the surface. Below the needle tip, there was a greater loss and greater return of hydrophobicity. According to Hillborg and Gedde [43], modest mechanical stress might cause the hydrophilic layer to crack, which leads to a quicker recovery. Gubanski [44] hypothesized that electrical discharge-induced deformation of the PDMS surface starts the angle recovery process at a faster rate. Moreover, at high humidity levels, the increase in oxygen content and silicone content was noticed, which can be attributed to the movement of LMWs from the bulk to the surface and also showed oxidation on the surface. The elemental composition of all samples under different operational conditions noticed an increase in oxygen level due to oxidation, an increase of silicone content due to the movement of LMWs to the surface, and a decrease in the filler content and carbon content due to the synergistic impact of stresses. FTIR results of micro-filler, nano-filler, and co-filled samples showed the better discharge resistance of co-filled composites under UV exposure and humidity. The formation of OH groups was visible in the FTIR spectra, suggesting the higher intensity of electrical stress along with other environmental stresses. The decrease in $SiCH_3$ peaks of sample R_2 was the highest, showing the loss of hydrophobicity, which is validated with the results of hydrophobicity and recovery.

5 Conclusions

In this study, electrical discharges were applied to six different types of composites for 100 h under different environmental stresses. The fillers used were ATH and MH with 50% micro-, 10% nano-, and 5% nano-/25% micro-concentrations. Different diagnostic techniques were employed to see the impact of stresses and electrical discharges on the surface of prepared composites. Hydrophobicity recovery was studied after different intervals of time and noticed that after 100 h of recovery, the contact angle did not reach 90° for each sample treated under different conditions. The samples having micro-fillers of 50% showed the slowest recovery because of the higher filler concentration that restricts the movement of LMWs to the surface of samples. The co-filled sample R_5 had the highest contact angle of 78.9° at high humidity without UV after 100 h of recovery. Sample R_1 filled with only micro-filler recorded the least recovery in the contact angle at the end of 100 h. Moreover, ATH-filled composites showed better results than those of MH, regardless of the concentration of fillers. The treated surface of samples R_5 and R_6 co-filled with two fillers showed better surface morphology than those of samples filled with only micro- and nano-filled composites. SEM micrographs for treated areas of R_1 and R_2 showed much more cracks and white powder on their surface under the impact of UV radiation. However, the surface just below the needle tip of samples R_5 and R_6 had better surface morphology. The elemental composition of all composites showed a decrease in filler concentrations, which are attributed to the impact of electrical discharges and synergistic stresses on the molecular structure of samples. As the severity of stresses increased, the oxygen percentage and silicone percentage also increased, which shows the formation of the oxidation process on the surface of samples, and the movement of LMWs to the surface was recorded. The formation of OH groups also shown in FTIR curves validates the process of oxidation due to the severity of electrical stress, UV, and high humidity. The loss of hydrophobicity can also be attributed to the loss of peaks of CH_3 methyl groups shown in FTIR spectra. In all cases, the co-filled sample R_5 having 5% nano-ATH and 25% micro-ATH performed better than other samples filled with micro- and nano-fillers. The co-filled composites R_5 and R_6 showed higher resistance to electrical discharges, UV, and humidity than the samples R_1, R_2, R_3, and R_4. This study contributes significantly to the understanding of the complex interplay between filler types, concentrations, and aging stresses in SR composites. The findings not only enhance our knowledge of material behavior under challenging environmental conditions but also pave the way for the development of more resilient and durable composite materials.

Acknowledgments: This work was supported by the 2022 Guilin Key R&D Plan Project (20220106-3) and 2022 Yulin City Central Leading Local Science and Technology Development Special Fund Project (20223402). This work was funded by the Researchers Supporting Project Number (RSPD2024R645) King Saud University, Riyadh, Saudi Arabia.

Funding information: This work was funded by the Researchers Supporting Project Number (RSPD2024R645) King Saud University, Riyadh, Saudi Arabia.

Author contributions: All authors have accepted responsibility for the entire content of this manuscript and approved its submission.

Conflict of interest: The authors state no conflict of interest.

Data availability statement: The datasets generated and/or analyzed during the current study are available from the corresponding author on reasonable request.

References

[1] Gubanski SM, Dernfalk A, Andersson J, Hillborg H. Diagnostic methods for outdoor polymeric insulators. IEEE Trans Dielectr Electr Insul. 2007 Oct;14(5):1065–80.

[2] Xu X, Dong Y, Hu Q, Si N, Zhang C. Electrochemical hydrogen storage materials: state-of-the-art and future perspectives. Energy Fuels. 2024 Apr;38(9):7579–613.

[3] Nazir MT, Xingliang J, Akram S. Laboratory investigation on hydrophobicity of new silicon rubber insulator under different environmental conditions. Dimensions. 2012;60(7):1–8.

[4] Hergert A, Kindersberger J, Bär C, Bärsch R. Transfer of hydrophobicity of polymeric insulating materials for high voltage outdoor application. IEEE Trans Dielectr Electr Insul. 2017 Apr;24(2):1057–67.

[5] Swift DA, Spellman C, Haddad A. Hydrophobicity transfer from silicone rubber to adhering pollutants and its effect on insulator performance. IEEE Trans Dielectr Electr Insul. 2006 Aug;13(4):820–9.

[6] Banik A, Mukherjee A, Dalai S. Development of a pollution flashover model for 11 kV porcelain and silicon rubber insulator by using COMSOL multiphysics. Electr Eng. 2018 Jun;100:533–41.

[7] Gubanski SM. Erosion resistance of different housing materials to UV irradiation and surface discharges action. In 1988 fifth international conference on dielectric materials, measurements and applications. IET; 1988 Jun. p. 37–40.

[8] Lan L, Yao G, Wang HL, Wen XS, Liu ZX. Characteristics of corona aged Nano-composite RTV and HTV silicone rubber. In 2013 Annual Report Conference on Electrical Insulation and Dielectric Phenomena. IEEE; 2013 Oct. p. 804–8.

[9] Venkatesulu B, Thomas MJ. Long-term accelerated weathering of outdoor silicone rubber insulators. IEEE Trans Dielectr Electr Insul. 2011 Mar;18(2):418–24.

[10] Haddad G, Gupta RK, Wong KL. Visualization of multi-factor changes in HTV silicone rubber in response to environmental exposures. IEEE Trans Dielectr Electr Insul. 2014 Oct;21(5):2190–8.

[11] Gorur R, Cherney E, Burnham J. Outdoor insulators. Phoenix, Arizona, USA: Ravi s. gorur. Inc. 1999. p. 179Y204.

[12] Phillips AJ, Childs DJ, Schneider HM. Water drop corona effects on full-scale 500 kV non-ceramic insulators. IEEE Trans Power Deliv. 1999 Jan;14(1):258–65.

[13] Sarathi R, Mishra P, Gautam R, Vinu R. Understanding the influence of water droplet initiated discharges on damage caused to corona-aged silicone rubber. IEEE Trans Dielectr Electr Insul. 2017 Sep;24(4):2421–31.

[14] Chen J, Davidson JH. Model of the negative DC corona plasma: Comparison to the positive DC corona plasma. Plasma Chem Plasma Process. 2003 Mar;23:83–102.

[15] Yang Z, Chen C, Li D, Wu Y, Geng Z, Konakov V, et al. An additively manufactured heat-resistant Al-Ce-Sc-Zr alloy: microstructure, mechanical properties and thermal stability. Mater Sci Eng: A. 2023 May;872:144965.

[16] Eifert A, Baier T, Hardt SJ. Small onset voltages in negative corona discharges using the edges of gold and aluminum foils as nano-structured electrodes. Appl Phys Lett. 2013 Jul;103(2):1–4.

[17] Simpson RB, editor. Rubber basics. UK: iSmithers Rapra Publishing; 2002.

[18] Yi F, Xu W, Yao X, Gong N, Zhang D, Du Z, et al. Study about the surface charge accumulation and dissipation of insulators under corona condition. In International Symposium on Insulation and Discharge Computation for Power Equipment. Singapore: Springer Nature Singapore; 2023 May. p. 445–56.

[19] Gao Y, Liang X, Dissado LA, Dodd SJ, Chalashkanov NM. Dielectric response of filled high temperature vulcanized silicone rubber. IEEE Trans Dielectr Electr Insul. 2016 Dec;23(6):3683–95.

[20] Ullah R, Akbar M, Amin S. Measuring electrical, thermal and mechanical properties of DC-stressed HTV silicone rubber loaded with nano/micro-fillers exposed to long-term aging. Appl Nanosci. 2020 Jul;10(7):2101–11.

[21] Khan H, Mahmood A, Ullah I, Amin M, Nazir MT. Hydrophobic, dielectric and water immersion performance of 9000 h multi-stresses aged silicone rubber composites for high voltage outdoor insulation. Eng Fail Anal. 2021 Apr;122:105223.

[22] Mahmood A, Alam S. Performance evaluation of micro/nano-silica filled silicone rubbers aged under multiple environmental stresses and bipolar DC voltage. J Rubber Res. 2023 Feb;26(1):55–70.

[23] Zhu Q, Chen J, Gou G, Chen H, Li P. Ameliorated longitudinal critically refracted—Attenuation velocity method for welding residual stress measurement. J Mater Process Technol. 2017 Aug;246:267–75.

[24] Ullah I, Akbar M, Khan HA. Degradation analysis of RTV-SiR based composites under both polarities DC voltage for insulators coating. Mater Today Commun. 2021 Dec;29:102890.

[25] Ullah I, Akbar M. Anti-aging characteristics of RTV-SiR aided HV insulator coatings: Impact of DC polarity and fillers. Mater Chem Phys. 2022 Feb;278:125634.

[26] Nazir MT, Phung BT, Yu S, Li S. Resistance against AC corona discharge of micro-ATH/nano-Al2O3 co-filled silicone rubber composites. IEEE Trans Dielectr Electr Insul. 2018 Apr;25(2):657–67.

[27] Nazir MT, Phung BT. AC corona resistance of micro-ATH/nano-Al 2 O 3 filled silicone rubber composites. In 2016 IEEE International Conference on High Voltage Engineering and Application (ICHVE). IEEE; 2016 Sep. p. 1–4.

[28] Meyer LH, Cherney EA, Jayaram SH. The role of inorganic fillers in silicone rubber for outdoor insulation alumina tri-hydrate or silica. IEEE Electr Insul Mag. 2004 Aug;20(4):13–21.

[29] Nazir MT, Phung BT, Yu S, Li S. Effects of thermal properties on tracking and erosion resistance of micro-ATH/AlN/BN filled silicone rubber composites. IEEE Trans Dielectr Electr Insul. 2018 Dec;25(6):2076–85.

[30] Ghunem RA, Ilhan S, Uckol HI, Tuzun D, Hadjadj Y. Viability of fillers in HTV silicone rubber in the AC and DC inclined plane tests. IEEE Trans Dielectr Electr Insul. 2021 Dec;28(6):2144–51.
[31] Ramirez I, Cherney EA, Jarayam S. Comparison of the erosion resistance of silicone rubber and EPDM composites filled with micro silica and ATH. IEEE Trans Dielectr Electr Insul. 2012 Feb;19(1):218–24.
[32] Ghunem RA, El-Hag AH, Hadjadj Y, Cherney EA. A study on the effect of inorganic fillers on the dry-band arcing erosion of silicone rubber composites. In 2017 IEEE Conference on Electrical Insulation and Dielectric Phenomenon (CEIDP). IEEE; 2017 Oct. p. 664–7.
[33] Reddy BS, Prasad DS. Effect of coldfog on the corona induced degradation of silicone rubber samples. IEEE Trans Dielectr Electr Insul. 2015 Jun;22(3):1711–8.
[34] Reddy BS. Corona degradation of the polymer insulator samples under different fog conditions. IEEE Trans Dielectr Electr Insul. 2016 Feb;23(1):359–67.
[35] Du BX, Xu H, Liu Y. Effects of wind condition on hydrophobicity behavior of silicone rubber in corona discharge environment. IEEE Trans Dielectr Electr Insul. 2016 Feb;23(1):385–93.
[36] Hakami M. Effects of corona discharges on silicone rubber samples under severe environmental conditions. Master's thesis. Canada: University of Waterloo.
[37] Hakami M, El-Hag A, Jayaram S. Effects of corona discharges on silicone rubber samples under severe weather conditions. In 2021 IEEE Electrical Insulation Conference (EIC). IEEE; 2021 Jun. p. 486–9.
[38] Nekeb A. Effect of some of climatic conditions in the performance of outdoor HV silicone rubber insulators. Doctoral dissertation. UK: Cardiff University.
[39] Stalder AF, Melchior T, Müller M, Sage D, Blu T, Unser M. Low-bond axisymmetric drop shape analysis for surface tension and contact angle measurements of sessile drops. Colloids Surf A: Physicochem Eng Asp. 2010 Jul;364(1–3):72–81.
[40] Saleem MZ, Akbar M. Review of the performance of high-voltage composite insulators. Polymers. 2022 Jan;14(3):431.
[41] Standard I. High-voltage test techniques: partial discharge measurements. IEC-60270. Switzerland: International Electrotechnical Commission; 2000. p. 13–31.
[42] Hillborg H, Gedde UW. Hydrophobicity changes in silicone rubbers. IEEE Trans Dielectr Electr Insul. 1999 Dec;6(5):703–17.
[43] Hillborg H, Gedde UW. Hydrophobicity recovery of polydimethylsiloxane after repeated exposure to corona discharges. Influence of crosslink density. In 1999 Annual Report Conference on Electrical Insulation and Dielectric Phenomena (Cat. No. 99CH36319). Vol. 2, IEEE; 1999 Oct. p. 751–5.
[44] Gubanski SM. Modern outdoor insulation-concerns and challenges. IEEE Electr Insul Mag. 2005 Nov;21(6):5–11.